Thermochimica Acta 476 (2008) 1–10

Contents lists available at ScienceDirect

Thermochimica Acta

journal homepage: www.elsevier.com/locate/tca

Differential approach for dynamic analysis to initial onset in heat flow rate spectroscopy of differential scanning calorimeter

Yu-Chu M. Li*

Department of Mechanical Engineering, Southern Taiwan University, #1 Nantai Street, Yongkang, Tainan 710, Taiwan, ROC

ARTICLE INFO

Article history:
Received 3 March 2008
Received in revised form 10 June 2008
Accepted 24 June 2008
Available online 10 July 2008

Keywords:
Extrapolated onset
Heat flow rate
Delay function
Moving interface

ABSTRACT

A differential approach is proposed for the determination of initial onset in differential scanning calorimeter (DSC) diagram of phase change material (PCM). By dissecting the spacing between extrapolated onset determined with traditional method and origin attributes to various delay mechanisms. A position-dependent term added into the traditional energy change equation accounts for thermal delay from any moving interfaces between separated phases of PCM inside a DSC cell pan. With the aid of Euler's equation in calculus of variations, the heat flow rate equation in relation to three major delay functions and temperature is formulated using chain rule of variables. The second-order differential operation with regard to heat flow rate in DSC diagram helps shortening the distance from extrapolated onset to origin, so as to initial onset can accurately located. The rampant fluctuation in the second-order derivative of heat flow rate in DSC diagram vindicates inadequate compensation of control unit in DSC, a result of serious feedback delay due to poor thermal conductivity and large latent heat in PCM.

1. Introduction

A differential scanning calorimeter (DSC) is instrumental in investigating thermal properties of phase change materials (PCMs) [1–2]. In practice, a poor assumption in solution [3] may result into inaccurate determination of thermal properties, such as melting point, latent heat, and specific heat. Although numerous test techniques and calibration standards were reported and improvements of the measurement uncertainty of DSC [4–7] were made, accurate determination of onset temperature, an element crucial to phase change, remained unsatisfactory. According to Höhne et al. [10], a true phase change temperature is associated with extrapolated onset temperature (T_e), heating rate β, and certified temperature (T_{cert}) of liquefaction under near equilibrium conditions. This sophisticated method is accurate, but not suitable for lay person. Per ISO 11357-1 and ISO 11357-3 [8,9], initial onset T_{im} for endothermic and exothermic effects due to changes in enthalpy depends on the temperature at which the test sample begins to melt. This temperature point is also the lower integration limit of enthalpy determination. It is likely that noise may smear the baseline temperature. This brings the challenge how to accurately determine the initial onset.

For the routine measurements in a DSC cell pan, prior studies assume a uniformly spaced phase change material (PCM). In fact, spatial uniformity between initial onset and final endset is hardly achieved due to the formation of moving interface(s) between separated phases in PCM. A novel technique [6] utilizing temperature-modulated differential scanning calorimeter (TMDSC) demonstrated a significant change in thermal resistance as a result of thickness of test sample and separation of polymer layers. Theoretically a thermal resistance would elongate the detection limit of initial onset. This method is therefore not very effective for the understanding of the impact from thermal delay mechanism to the detection accuracy of initial onset. Effect of thermal delay on the determination of initial onset due to moving interface(s) in PCM requires more systematic studies. Charsley et al. [4], utilized a stepwise heating procedure with a partially melting method on several organic melting temperature standards. However, the existence of at least one discontinuity between separated phases in PCM during partially melting was still addressed. During any stepwise heating in partially melting conditions, one liquid zone may form within the solid phase of a test sample. Two moving interfaces (i.e., solid–liquid interface and liquid–solid interface) may be observed due to partially melting in stepwise heating. The fixed contact interface appears between the metallic bottom of a DSC cell pan

* Tel.: +886 6 2533131x3546; fax: +886 6 2425092.
E-mail address: maxli@mail.stut.edu.tw.

0040-6031/$ – see front matter © 2008 Elsevier B.V. All rights reserved.
doi:10.1016/j.tca.2008.06.016

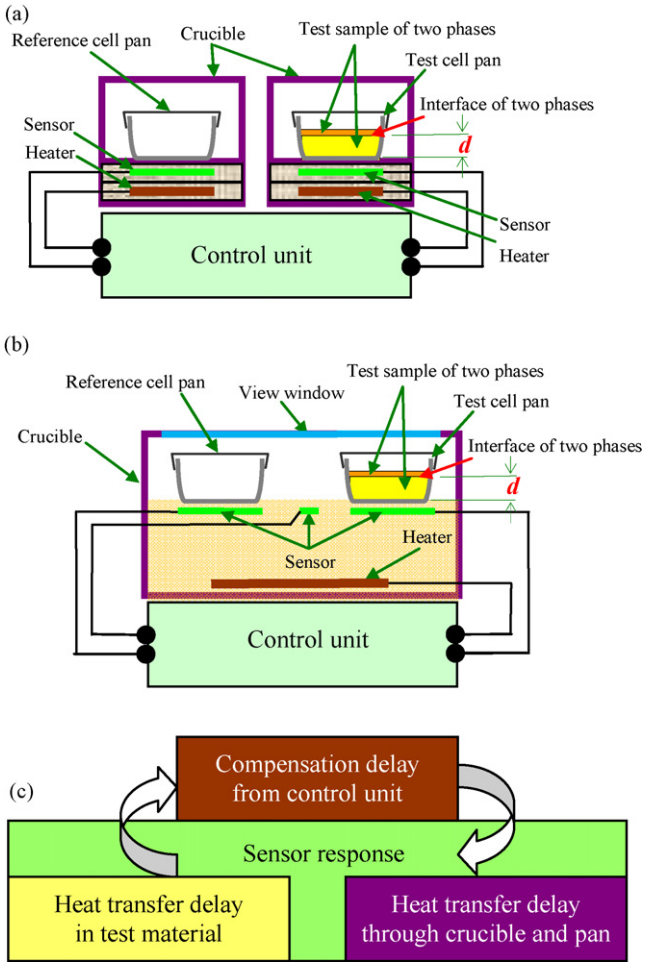

Fig. 1. Major delay sources in different schematic DSC configuration plots for (a) a typical heat-compensated DSC, and (b) a typical heat-flux DSC, as well as (c) their delay chain diagram.

and the test sample, and any moving interface(s) exists between the top of the test sample and the ambient gas sealed in the DSC cell pan. In addition, thermal conductivity and heat capacities may also cause variations of heat transfer during DSC measurements.

Between test sample and temperature sensor, as shown in Fig. 1 schematically, temperature gradient $\vec{\nabla}T$ always present due to thermal resistance. The initial onset will show phase lags at the temperature change of test sample. Martins and Cruz-Pinto [5], demonstrated a constant extrapolated onset if a scan rate was kept small enough. This suggests that initial onset may be determined by the same way. Thus, a variational calculus approach to determine an accurate initial onset can be free from tempering of the baseline by noise. We therefore realized the thermal behavior of separated phases within PCM encapsulated inside a DSC cell pan.

2. Theory

2.1. Energy change equation

Many attributes contribute to the determination of initial onset and extrapolated onset Major sources of errors include heater geometry, heating rate/procedure, accuracy/geometry of temperature sensor, geometry/thermal properties of crucible, specimen preparation, specimen mass/geometry, geometry/thermal properties of cell pan, geometry/thermal properties of moving interface in specimen, purge gas flow, type of purge gas, electronic feedback control, starting/end temperature, etc. In order to capture the overall delay effect of moving interface(s) between spatially separated phases of a test sample, the governing equation for the energy change of the test sample encapsulated inside a DSC cell pan is as follows:

$$\delta Q_{\mathrm{PCM}} = \left(\frac{\partial H}{\partial p} - V\right)_{T,n} \mathrm{d}p + \left[\left(\frac{\partial H}{\partial T}\right)_{p,n} \mathrm{d}T + \left(\frac{\partial H}{\partial n}\right)_{p,T} \mathrm{d}n\right] + (\vec{\nabla}H)_{p,n} \cdot \mathrm{d}\vec{r} - \sum_{n} \mathrm{d}E_n, \tag{1}$$

in which H is enthalpy function, n partition of phase change in PCM, p pressure, V volume of PCM, T temperature, $\vec{r}$ position vector and E_n various forms of energy. Two parts of the second term in the Eq. (1) correspond to sensible heat and latent heat of PCM, respectively, usually measured under extremely slow heat transfer rate near thermal equilibrium. The third term describes energy variation due to the spatial effect between temperature sensor in DSC and moving interface(s) of separated phases within PCM.

In case that $\vec{\nabla}T$ is kept infinitesimal everywhere during phase change, a uniform phase change temperature condition in fixed-point cells for primary temperature calibration, the third term may be dropped out. In the routine measurement process of DSC, the temperature change, either rising or descending, however, is big enough for the consideration of measurement accuracy of heat flow rate, which is a derived quantity of temperature and time. Using a variable change in the third term under the principle of chain rule, the Eq. (1) may be rewritten as

$$\begin{aligned}\delta Q_{\mathrm{PCM}} &= \left(\frac{\partial H}{\partial p} - V\right)_{T,n} \mathrm{d}p + \left[\left(\frac{\partial H}{\partial T}\right)_{p,n} \mathrm{d}T + \left(\frac{\partial H}{\partial n}\right)_{p,T} \mathrm{d}n\right] + \left(\frac{\partial H}{\partial T}\vec{\nabla}T\right)_{p,n} \cdot \mathrm{d}\vec{r} - \sum_n \mathrm{d}E_n \\ &= \left(\frac{\partial H}{\partial p} - V\right)_{T,n} \mathrm{d}p + \left[\left(\frac{\partial H}{\partial T}\right)_{p,n} \mathrm{d}T + \left(\frac{\partial H}{\partial n}\right)_{p,T} \mathrm{d}n\right] \\ &\quad - \frac{\partial H}{\partial T}\left\{\frac{[(1-\mathrm{e}^{-t/\tau_{\mathrm{AC}}})\cdot(1-\mathrm{e}^{-t/\tau_{\mathrm{TH}}})\cdot(1-\mathrm{e}^{-t/\tau_{\mathrm{MI}}})\cdot(-A_{\mathrm{PCM}}k\vec{\nabla}T)]}{[(1-\mathrm{e}^{-t/\tau_{\mathrm{AC}}})\cdot(1-\mathrm{e}^{-t/\tau_{\mathrm{TH}}})\cdot(1-\mathrm{e}^{-t/\tau_{\mathrm{MI}}})\cdot(A_{\mathrm{PCM}}k)]}\right\}_{p,n} \mathrm{d}\vec{r} - \sum_n \mathrm{d}E_n,\end{aligned} \tag{2}$$

where t is test time, τ_{AC} automatic control delay constant, τ_{TH} thermal delay constant, τ_{MI} moving interface delay constant, k thermal conductivity of PCM, and A_{PCM} area of heat transfer in PCM. The term, $(-A_{\mathrm{PCM}}k\vec{\nabla}T)$, describes the heat flow rate from the heater inside a crucible to PCM via the wall of the DSC cell pan. A simplified delay function, $(1-\mathrm{e}^{-t/\tau_{\mathrm{AC}}})$, of automatic control delay constant τ_{AC}, reflects the compensation delay owing to electronic feedback control from control unit of DSC, following an abrupt change of enthalpy like a delta function as either melting or freezing happens. A simplified delay function, $(1-\mathrm{e}^{-t/\tau_{\mathrm{TH}}})$, of thermal delay constant τ_{TH}, represents the heat transfer delay through fixed parts, i.e., the crucible and DSC cell pan, in DSC. Once melting (freezing) starts, the formed moving interface(s) between separated liquid and solid phases in PCM drifts away from the bottom of the DSC cell pan. Therefore, $(1-\mathrm{e}^{-t/\tau_{\mathrm{MI}}})$, a simplified delay function of moving interface delay constant τ_{MI}, stands for the heat transfer delay mainly from the bottom of the crucible to the moving interface(s) via the wall of the DSC cell pan.

2.2. Total enthalpy change of complete phase change

After tedious derivation and with the aid of calculus of variation, we can achieve the effective heat flow rate of 3D configuration, $\bar{q}$, as presented in Appendix. Because $\bar{q}$ is a position function concerning moving interface(s) between separated phases in PCM, the total enthalpy change of complete phase change from initial onset to final endset may be evaluated through the integral of $\bar{q}$ over time:

$$\begin{aligned}\Delta Q_{\mathrm{PCM}} &= \int_{t_{\mathrm{Onset}}}^{t_{\mathrm{Endset}}} \bar{q}\ \mathrm{d}t \\ &= \int_{t_{\mathrm{Onset}}}^{t_{\mathrm{Endset}}} \bar{q}\ \mathrm{d}(C_T T) \\ &= C_T \int_{t_{\mathrm{Onset}}}^{t_{\mathrm{Endset}}} \mathrm{d}T \left[-C_{\mathrm{delay}} \times \left(A_{x,\mathrm{PCM}}k\frac{T_{x,\mathrm{PC}} - T_{x,\mathrm{pan}}}{\Delta x}\right) \times \left(A_{y,\mathrm{PCM}}k\frac{T_{y,\mathrm{PC}} - T_{y,\mathrm{pan}}}{\Delta y}\right) \times \left(A_{z,\mathrm{PCM}}k\frac{T_{z,\mathrm{PC}} - T_{z,\mathrm{pan}}}{\Delta z}\right)\right]^{1/3}\end{aligned} \tag{3}$$

In the Eq. (3), C_T is the reciprocal of scan rate, and C_{delay} stands for the total effective delay function defined in Appendix. $T_{x,\mathrm{pan}}$, $T_{y,\mathrm{pan}}$ and $T_{z,\mathrm{pan}}$ stand for inner crucible temperatures in x-, y- and z-direction, respectively under the bottom of the DSC cell pan, monitored by a temperature sensor, which is embedded in the bottom of the crucible. $T_{x,\mathrm{PC}}$, $T_{y,\mathrm{PC}}$ and $T_{z,\mathrm{PC}}$ indicate moving interface temperatures in x-, y- and z-direction, respectively between separated phases within PCM. $A_{x,\mathrm{PCM}}$, $A_{y,\mathrm{PCM}}$ and $A_{z,\mathrm{PCM}}$ represent different areas of heat transfer normal to x-, y- and z-direction in PCM, respectively.

According to the Eq. (3), the greater latent heat a test sample may possess, the larger the difference between the constant phase change temperature of moving interface in the test sample and the temperature measured by the temperature sensor can become. This is conformable with the well-known broadening phenomenon of phase change peak due to large mass of test sample.

3. Experimental

The instrument studied in this work was a heat-compensated PerkinElmer DSC 7, which was routinely calibrated according to the calibration procedure using an indium standard (Product#: 0219–1207, Feb/2003), from PerkinElmer Inc., with a purity of 99.999%, and a mass of 5.911 mg was sealed in an aluminum DSC cell pan. A distilled water sample with a mass of 9.4 mg was also sealed in an aluminum DSC cell pan identical to that used for the indium standard sample. The experiment was performed with scan rate of +5 °C/min under nitrogen purge gas flow.

4. Results and discussions

4.1. Predicted response

An ideal melting process may be simulated by a delta function of unity area with an infinitesimal temperature interval δT. On both sides of melting points, sensitive heat on which latent heat may be superimposed is usually discontinuous. To simplify the analysis, sensitive heat may be treated as a background, and thus subtracted from the DSC curve. However, it is not possible to have a response curve like a delta function of unity area with an infinitesimal temperature interval δT in practical DSC measurements. Anyway, we may adopt a rectangular function of unity area, as schematically shown in Fig. 2(a), to approximate a melting process under the constant heat flow rate of magnitude $1/\Delta T$ within a finite temperature interval ΔT. To adjust the response magnitude regarding the simple delay function $(1-\mathrm{e}^{-C_T T/\tau})$ and the

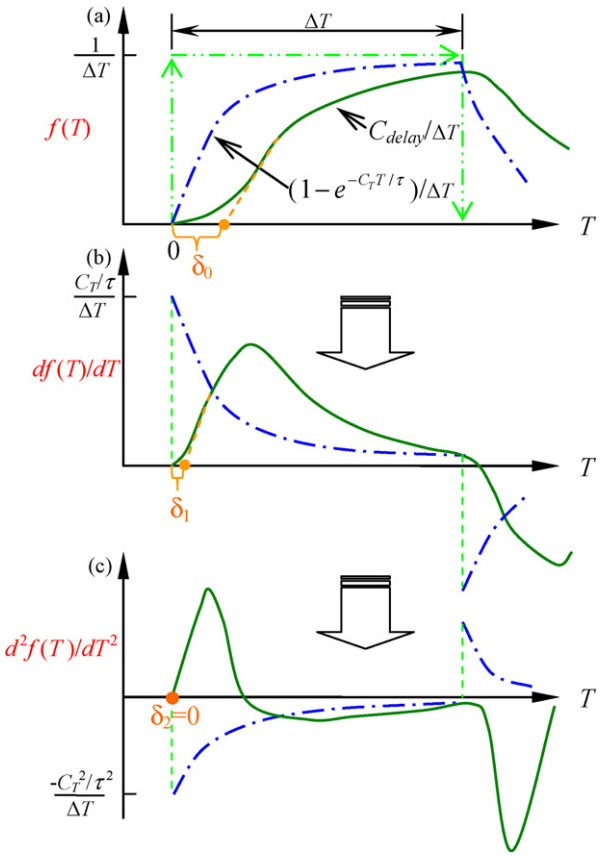

Fig. 2. Schematic plot of response: (a) two delay functions responding to a rectangular function of unity area, (b) their first-order derivatives, and (c) second-order derivatives. (δ_0, δ_1, and δ_2: offset of extrapolated onset).

total effective delay function C_{delay} to the rectangular function of unity area, the factor $1/\Delta T$ is multiplied to each function. Clearly illustrated in Fig. 2(a), the offset δ_0 reflects the distance from extrapolated onset to origin for the adjusted total effective delay function $C_{\text{delay}}/\Delta T$, while there is no offset at all for the adjusted simple delay function $(1 - e^{-C_T T/\tau})/\Delta T$. After the first-order differential operation to the adjusted total effective delay function $C_{\text{delay}}/\Delta T$ with respect to temperature T, the offset δ_0 is obviously greater than the offset δ_1, shown in Fig. 2(b). Furthermore, after the second-order differential operation to the adjusted total effective delay function $C_{\text{delay}}/\Delta T$ with respect to temperature T, the offset δ_2, illustrated in Fig. 2(c), becomes zero exactly. Since the offset obtained from extrapolation operation can be reduced by differential methods, this approach may be suitable for heat flow rate in DSC diagram.

Supposed that all heat flow rates in x-, y-, and z-direction to a homogeneous PCM are isotropic and identical delay parameters, the Eq. (A.15) may be reduced to the simple form $(1 - e^{-C_T T/\tau})^3$. As illustrated in the top of Fig. 3 schematically, three delay functions of distinct exponents (I, II and III) corresponding to a step function of unity height and their derivatives with respect to temperature T behave quite different near origin. After differentiation twice to the simple form $(1 - e^{-C_T T/\tau})^3$ with respect to temperature T, the offset from extrapolated onset to origin, as shown in the bottom-right of Fig. 3, can be eliminated fully, so as to achieve initial onset, i.e., the origin point.

4.2. Offset analysis of DSC test results

As shown in Fig. 4(a) and (b), both black curves in DSC diagrams represent the same measured heat flow rate of the water sample. In Fig. 4(a), the pink curve stands for the first-order derivative of the measured heat flow rate. The difference between the extrapolated onset determined via traditional method [8–10] and that from the first-order derivative of the measured heat flow rate is about 0.4 °C. In Fig. 4(b), a pink curve fluctuating sharply is the second-order derivative of the measured heat flow rate. To make the evaluation of extrapolated onset easy, a low-pass filtration to the fluctuation of the pink curve results in a dot black curve, shown in Fig. 4(b). Hence, the subsequent second-order differential operation to the measured heat flow rate extends the difference between the extrapolated onset determined with traditional method and that achieved by this second-order differential method to roughly 0.9 °C.

The sharp fluctuation away from initial onset in the second-order derivative of the measured heat flow rate was probably caused by the coupling effect of poor thermal conductivity and large latent heat in the water sample. To vindicate the coupling effect of thermal conductivity and latent heat, we chose indium, used as the calibration standard, for comparison. In fact, thermal conductivity of indium at melting point (72 W/m K) is much greater than that of water at melting point (0.56 W/m K) [11]. Indium at melting point (28.42 J/g) possesses much less latent heat than water at melting point (333.6 J/g). The fast feedback from excellent thermal conductance enables the control unit in DSC to catch up with the small energy demand of moving interface(s) in a melting indium, and thus effectively prohibits the rapid fluctuation of heat flow rate during DSC measurements. After the second-order differential operation to the

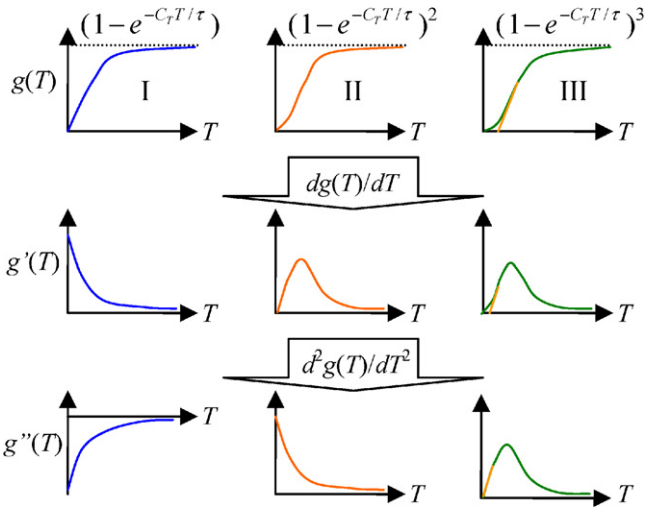

Fig. 3. Schematic plot of near-origin behavior for three different delay functions of distinct exponents respectively (I, II and III) responding to a step function of unity height and their derivatives with respect to temperature *T*.

measured heat flow rate curve, no significant fluctuation, as shown in Fig. 5, was observed and our presumption is validated only for water and indium. The coupling effect of poor thermal conductivity and large latent heat can result in serious feedback delay to the control unit in DSC. To mitigate this delay problem, a reduction of scan rates for the control unit in DSC allowing catch up in time may be an inevitable option. Besides, two more examples, paraffin wax (135 °F fully refined grade, Taiwan Wax Company Ltd., R.O.C.) and benzene (Riedel-deHaën 32212, Germany), were tested, as shown in Figs. 6 and 7. Since their thermal conductivities are less than that of water, the second-order derivatives of the measured heat flow rates with respect to temperature start fluctuating right from their initial onsets.

On examining those curves in the second-order derivatives as shown in Fig. 2(c), Fig. 4(b) and Fig. 5(b), their similarity of shape indicates that the exponential order of delay function should not be less than three. In accordance with the illustrations in Fig. 2(a)–(c), using the second-order differential operation to the adjusted total effective delay function $C_{\text{delay}}/\Delta T$ can eliminate the offset δ_0 from extrapolated onset to origin. However, there is still a tiny tail left in the second-order derivative of Fig. 5(b). Even in Fig. 5(c), the tiny tail cannot be removed completely. This suggests that eliminating the rest tiny tail requires higher order differential operation to the measured heat flow rate due to the fact that other important delay mechanisms were neglected in Fig. 1.

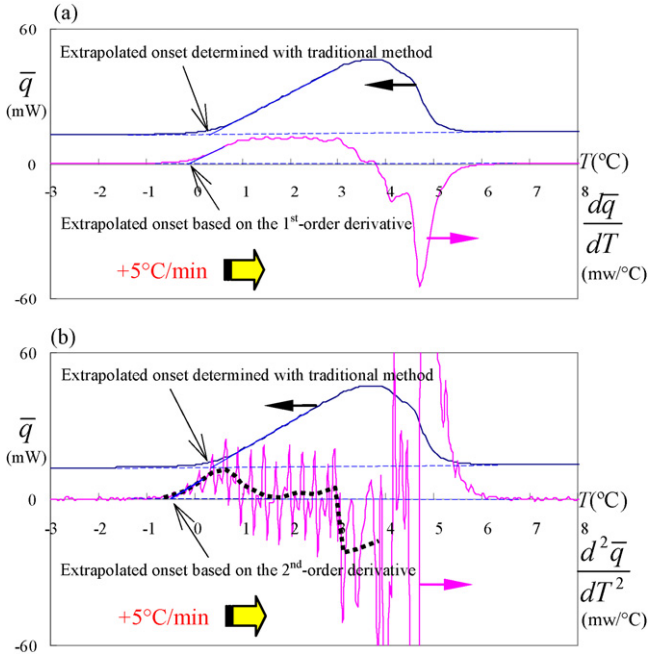

Fig. 4. Endothermic extrapolated onsets of the distilled water sample (9.4 mg) decided with traditional method and differential method respectively: (a) the first-order derivative of the heat flow rate with respect to temperature brings the extrapolated onset to the left by 0.5 °C; (b) the second-order derivative of the heat flow rate with respect to temperature further moves the extrapolated onset to the left by 0.9 °C (scan rate of PerkinElmer DSC 7: +5 °C/min). (For interpretation of the references to color in the citation of this figure, the reader is referred to the web version of the article.)

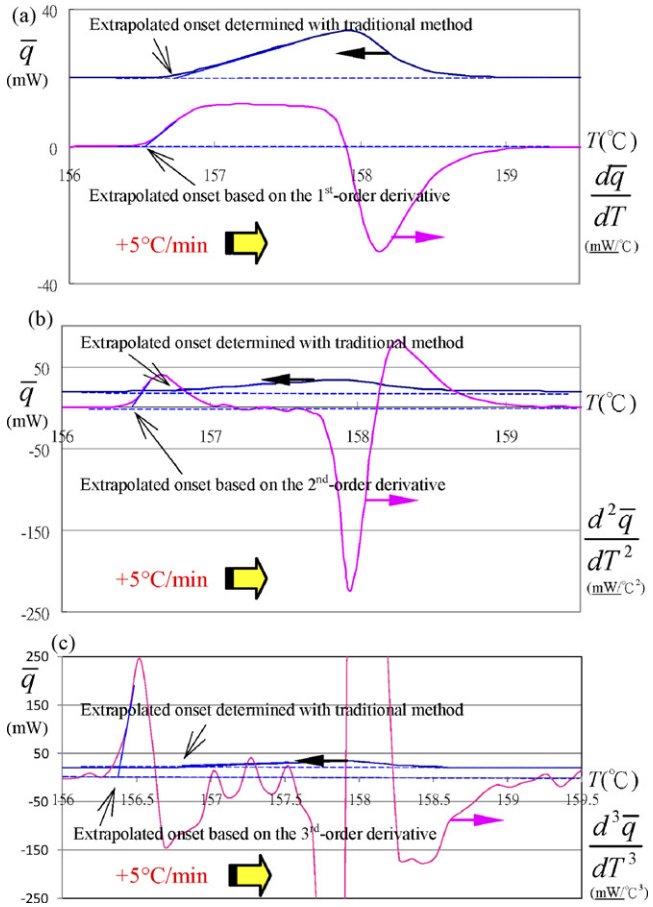

Fig. 5. Endothermic extrapolated onsets of the indium standard (5.911 mg, PerkinElmer Product #: 0219–1207, Feb/2003) decided with traditional method and differential method, respectively: (a) the first-order derivative of the heat flow rate with respect to temperature brings the extrapolated onset to the left by 0.09 °C; (b) the second-order derivative of the heat flow rate with respect to temperature further moves the extrapolated onset to the left by 0.17 °C (scan rate of PerkinElmer DSC 7: +5 °C/min).

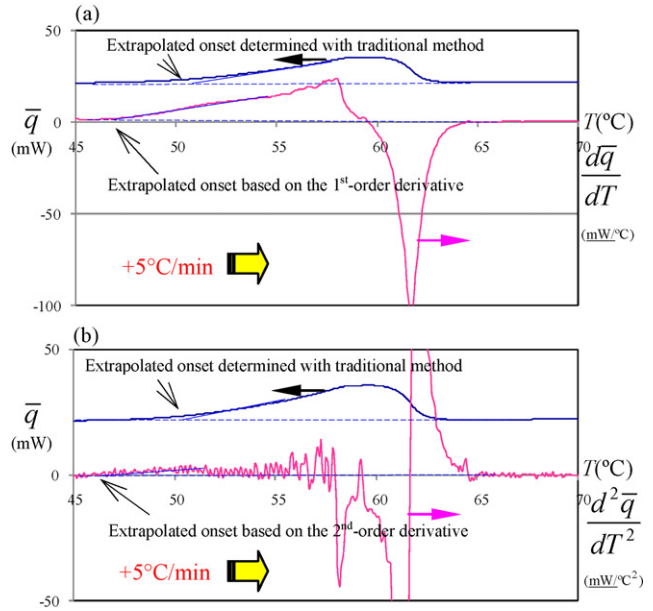

Fig. 6. Endothermic extrapolated onsets of the paraffin wax sample (7.5 mg, 135 °F fully refined grade, Taiwan Wax Company Ltd., R.O.C.) decided with traditional method and differential method respectively: (a) the first-order derivative of the heat flow rate with respect to temperature brings the extrapolated onset to the left by 0.09 °C; (b) the second-order derivative of the heat flow rate with respect to temperature further moves the extrapolated onset to the left by 0.17 °C (scan rate of PerkinElmer DSC 7: +5 °C/min).

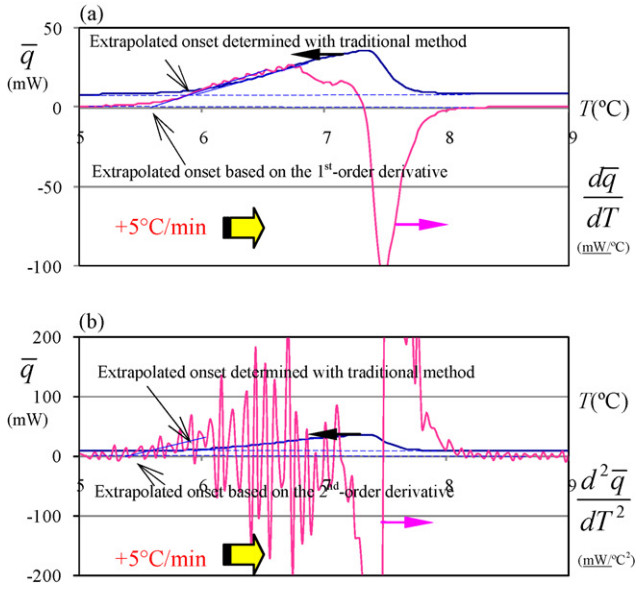

Fig. 7. Endothermic extrapolated onsets of the benzene sample (9.5 mg, Riedel-deHaën 32212, Germany) decided with traditional method and differential method respectively: (a) the first-order derivative of the heat flow rate with respect to temperature brings the extrapolated onset to the left by 0.09 °C; (b) the second-order derivative of the heat flow rate with respect to temperature further moves the extrapolated onset to the left by 0.17 °C (scan rate of PerkinElmer DSC 7: +5 °C/min).

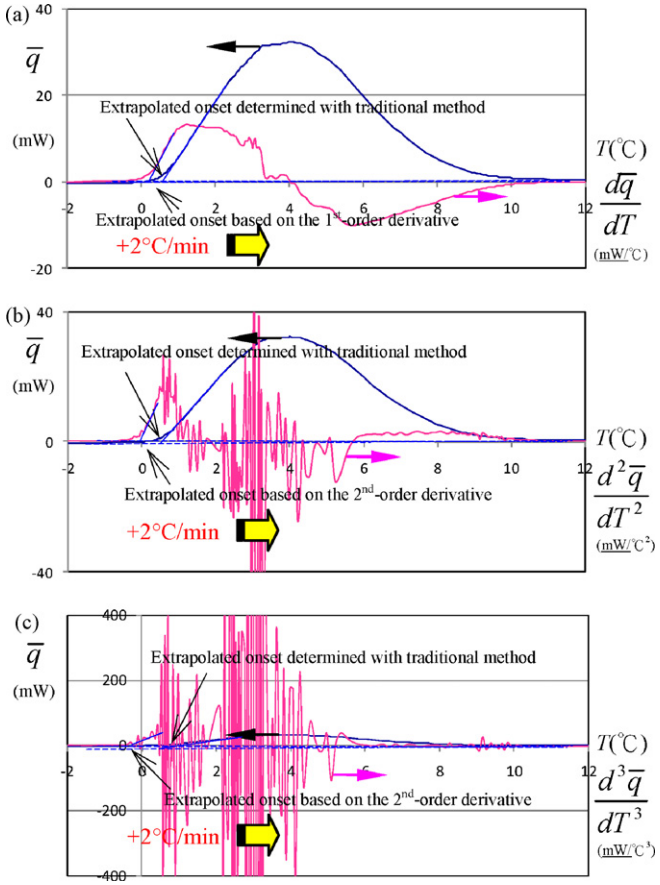

Fig. 8. Endothermic extrapolated onsets of the distilled water sample (12.5 mg) decided with traditional method and differential method respectively: (a) the first-order derivative of the heat flow rate with respect to temperature brings the extrapolated onset to the left by 0.5 °C; (b) the second-order derivative of the heat flow rate with respect to temperature further moves the extrapolated onset to the left by 0.9 °C (scan rate of Thermal Analysis (DuPont) DSC 2920: +2 °C/min).

To compare the difference between typical responses of heat flow rate heat-compensated DSC and heat-flux DSC, we applied a Thermal Analysis (DuPont) DSC 2920, which is a heat-flux type, to test a distilled water sample of 12.5 mg. Since the peak resolution of the Thermal Analysis (DuPont) DSC 2920 is inferior to that of the PerkinElmer DSC 7, reduction of the scan rate to +2 °C/min can achieve better peak resolution, and also lesser fluctuation of higher-order derivatives of heat flow rate due to improved feedback control under slower scan rate. This can be validated by the smoother curves near the initial onset in Fig. 8(b) and (c).

During reversible cycling DSC tests, initial onset drawn from endothermic curve must be equal to that from exothermic one, as expected in theory. However, for most PCMs, thermal conductivity of liquid phase is usually different from that of solid phase. Thus, endothermic curve becomes slightly asymmetric to exothermic one during reversible cycling DSC tests. Although reversible cycling DSC tests may give more information about tested materials, the supercooling effect during cooling scan process [5] can distort measured DSC curves seriously. To prevent such supercooling problem, heating scan process becomes a reliable choice owing to the fact that thermal agitation from heating action can trigger melting in tested materials.

5. Conclusions

In this work we formulated the heat flow rate equation consisting of three delay functions with calculus of variations. Differential operation to heat flow rate in DSC diagram can shorten the distance from extrapolated onset determined via traditional method to origin, i.e., initial onset. To totally eliminate this distance may require higher order differential operation in order to get rid of all possible delay effects on heat flow rate in DSC diagram. The rampant fluctuations in the second-order derivative of heat flow rate are results from the coupling effect of poor thermal conductivity and large latent heat. These effects cause serious feedback delay and the control unit in DSC cannot catch up for compensation in time. To mitigate this severe delay problem, a reduction of scan rate may be an inevitable option.

Acknowledgment

This research was financially supported by the National Science Committee in Taiwan (Grant number: NSC 95-2622-E-218-017-CC3).

Appendix A

Derivation of heat flow rate equation by calculus of variations

In accordance with the alternate form of Euler's equation regarding calculus of variations [12], the x-direction term, $\partial H/\partial x$ of $\vec{\nabla}H$ in the Eq. (1) can be expressed as

$$\frac{\partial H}{\partial x} = \frac{\mathrm{d}}{\mathrm{d}x}\left\{ H - \left[-(1-\mathrm{e}^{-t/\tau_{x,\mathrm{AC}}})\cdot(1-\mathrm{e}^{-t/\tau_{x,\mathrm{TH}}})\cdot(1-\mathrm{e}^{-t/\tau_{x,\mathrm{MI}}})\cdot\left(A_{x,\mathrm{PCM}}k\ \frac{\mathrm{d}T}{\mathrm{d}x}\right)\right] \times \frac{\partial H}{\partial\left[-(1-\mathrm{e}^{-t/\tau_{x,\mathrm{AC}}})\cdot(1-\mathrm{e}^{-t/\tau_{x,\mathrm{TH}}})\cdot(1-\mathrm{e}^{-t/\tau_{x,\mathrm{MI}}})\cdot\left(A_{x,\mathrm{PCM}}k\ \frac{\mathrm{d}T}{\mathrm{d}x}\right)\right]} \right\}. \tag{A.1}$$

For practical DSC measurements, $H = H(T, \mathrm{d}T/\mathrm{d}x)_p$, $\Delta T/\Delta t$, and x does not appear explicitly. Therefore, the Eq. (3) may be reduced to be

$$0 = \frac{\mathrm{d}}{\mathrm{d}x}\left\{ H - \left[-(1-\mathrm{e}^{-t/\tau_{x,\mathrm{AC}}})\cdot(1-\mathrm{e}^{-t/\tau_{x,\mathrm{TH}}})\cdot(1-\mathrm{e}^{-t/\tau_{x,\mathrm{MI}}})\cdot\left(A_{x,\mathrm{PCM}}k\ \frac{\mathrm{d}T}{\mathrm{d}x}\right)\right] \times \frac{\partial H}{\partial\left[-(1-\mathrm{e}^{-t/\tau_{x,\mathrm{AC}}})\cdot(1-\mathrm{e}^{-t/\tau_{x,\mathrm{TH}}})\cdot(1-\mathrm{e}^{-t/\tau_{x,\mathrm{MI}}})\cdot\left(A_{x,\mathrm{PCM}}k\ \frac{\mathrm{d}T}{\mathrm{d}x}\right)\right]} \right\}. \tag{A.2}$$

After integrating both sides over x, we obtain

$$C_x = H - \left[-(1-\mathrm{e}^{-t/\tau_{x,\mathrm{AC}}})\cdot(1-\mathrm{e}^{-t/\tau_{x,\mathrm{TH}}})\cdot(1-\mathrm{e}^{-t/\tau_{x,\mathrm{MI}}})\cdot\left(A_{x,\mathrm{PCM}}k\ \frac{\mathrm{d}T}{\mathrm{d}x}\right)\right] \times \frac{\partial H}{\partial[-(1-\mathrm{e}^{-t/\tau_{x,\mathrm{AC}}})\cdot(1-\mathrm{e}^{-t/\tau_{x,TH}})\cdot(1-\mathrm{e}^{-t/\tau_{x,MI}})\cdot(A_{x,\mathrm{PCM}}k(\mathrm{d}T/\mathrm{d}x)],} \tag{A.3}$$

in which C_x is a constant.

For simplicity, let's define the heat flow rate in x-direction as

$$q_x = -(1-\mathrm{e}^{-t/\tau_{x,\mathrm{AC}}})(1-\mathrm{e}^{-t/\tau_{x,\mathrm{TH}}})(1-\mathrm{e}^{-t/\tau_{x,\mathrm{MI}}})\left(A_{x,\mathrm{PCM}}k\ \frac{\mathrm{d}T}{\mathrm{d}x}\right). \tag{A.4}$$

Hence, the Eq. (A.2) can be put down as

$$\left(\frac{1}{q_x}\right)\partial q_x = \left[\frac{1}{H - C_x}\right]\partial H. \tag{A.5}$$

Dividing ∂T on both sides of the Eq. (A.5), we obtain

$$\left(\frac{1}{q_x}\right)\left(\frac{\partial q_x}{\partial T}\right) = \left[\frac{1}{H - C_x}\right]\left(\frac{\partial H}{\partial T}\right). \tag{A.6}$$

In case of approaching nearby of $H = C_x$, the predicted value of $(1/q_x)(\partial q_x/\partial T)$ diverges theoretically similar to the derivative of a delta function, although the derivative of heat flow rate derived from practical DSC measurement is always continuous.

Similarly, along y-direction we have

$$\left(\frac{1}{q_y}\right)\left(\frac{\partial q_y}{\partial T}\right) = \left[\frac{1}{H - C_y}\right]\left(\frac{\partial H}{\partial T}\right), \tag{A.7}$$

and along z-direction we get

$$\left(\frac{1}{q_z}\right)\left(\frac{\partial q_z}{\partial T}\right) = \left[\frac{1}{H - C_z}\right]\left(\frac{\partial H}{\partial T}\right). \tag{A.8}$$

Summing the Eqs. (A.6)–(A.8) up, we have

$$\left(\frac{1}{q_x}\right)\left(\frac{\partial q_x}{\partial T}\right) + \left(\frac{1}{q_y}\right)\left(\frac{\partial q_y}{\partial T}\right) + \left(\frac{1}{q_z}\right)\left(\frac{\partial q_z}{\partial T}\right) = \left[\frac{1}{H - C_x}\right]\left(\frac{\partial H}{\partial T}\right) + \left[\frac{1}{(H - C_y)}\right]\left(\frac{\partial H}{\partial T}\right) + \left[\frac{1}{H - C_z}\right]\left(\frac{\partial H}{\partial T}\right). \tag{A.9}$$

Putting the three terms in the left side of the Eq. (A.9) together, the following equation can be obtained:

$$\frac{\partial(\ln q_x + \ln q_y + \ln q_z)}{\partial T} = \partial\frac{[\ln(H - C_x) + \ln(H - C_y)\ln(H - C_z)]}{\partial T}. \tag{A.10}$$

Therefore,

$$\frac{\partial \ln(q_x q_y q_z)}{\partial T} = \frac{\partial \ln[(H - C_x)(H - C_y)(H - C_z)]}{\partial T}. \tag{A.11}$$

Integrating both sides of the Eq. (A.11) over T, the following equation can be rendered

$$q_x q_y q_z = C_0(H - C_x)(H - C_y)(H - C_z), \tag{A.12}$$

where C_0 is a constant. The form of $q_x q_y q_z$ is similar to the product in the method of separation of variables for solving partial differential equation in 3D configuration. Thus, we may define the effective heat flow rate of 3D configuration as follows:

$$\begin{aligned}\bar{q} &= \sqrt[3]{q_x q_y q_z} \\ &= \left\{ -[(1 - e^{-t/\tau_{x,AC}}) \cdot (1 - e^{-t/\tau_{x,TH}}) \cdot (1 - e^{-t/\tau_{x,MI}}) \cdot (1 - e^{-t/\tau_{y,AC}}) \cdot (1 - e^{-t/\tau_{y,TH}}) \cdot (1 - e^{-t/\tau_{y,MI}}) \right. \\ &\quad \left. \cdot (1 - e^{-t/\tau_{z,AC}}) \cdot (1 - e^{-t/\tau_{z,TH}}) \cdot (1 - e^{-t/\tau_{z,MI}})] \cdot \left(A_{x,PCM} k \frac{\partial T}{\partial x}\right) \cdot \left(A_{y,PCM} k \frac{\partial T}{\partial y}\right) \cdot \left(A_{z,PCM} k \frac{\partial T}{\partial z}\right) \right\}^{1/3} \\ &= \sqrt[3]{C_0(H - C_x)(H - C_y)(H - C_z)}\end{aligned} \tag{A.13}$$

During routine DSC measurements, the way of constant scan rate is most favored owing to its simplicity and ease for feedback control. That is, the temperature-changing rate $\Delta T/\Delta t$ is always kept constant during measurement. Therefore, let $t = C_T T$, where C_T is the reciprocal of scan rate. Then, we can write down the approximate form of the effective heat flow rate as

$$\begin{aligned}\bar{q} \approx \left\{ -[(1 - e^{-C_T T_{x,PC}/\tau_{x,AC}}) \cdot (1 - e^{-C_T T_{x,PC}/\tau_{x,TH}}) \cdot (1 - e^{-C_T T_{x,PC}/\tau_{x,MI}}) \cdot (1 - e^{-C_T T_{y,PC}/\tau_{y,AC}}) \cdot (1 - e^{-C_T T_{y,PC}/\tau_{y,TH}}) \cdot (1 - e^{-C_T T_{y,PC}/\tau_{y,MI}}) \right. \\ \cdot (1 - e^{-C_T T_{z,PC}/\tau_{z,AC}}) \cdot (1 - e^{-C_T T_{z,PC}/\tau_{z,TH}}) \cdot (1 - e^{-C_T T_{z,PC}/\tau_{z,MI}})] \\ \left. \cdot \left[\left(A_{x,PCM} k \frac{T_{x,PC} - T_{x,pan}}{\Delta x}\right) \cdot \left(A_{y,PCM} k \frac{T_{y,PC} - T_{y,pan}}{\Delta y}\right) \cdot \left(A_{z,PCM} k \frac{T_{z,PC} - T_{z,pan}}{\Delta z}\right)\right] \right\}^{1/3}.\end{aligned} \tag{A.14}$$

$T_{x,pan}$, $T_{y,pan}$ and $T_{z,pan}$ stand for inner crucible temperatures in x-, y- and z-direction, respectively under the bottom of the DSC cell pan, monitored by a temperature sensor, which is embedded in the crucible. For most commercial DSCs, each crucible protected with a lid/or view window is closely monitored using a temperature sensor only. Therefore, $T_{x,pan} = T_{y,pan} = T_{z,pan}$. On the other hand, $T_{x,PC}$, $T_{y,PC}$ and $T_{z,PC}$ indicate moving interface temperatures in x-, y- and z-direction, respectively between separated phases within PCM. Besides, for the convenience of further derivations, let C_{delay} stand for the total effective delay function:

$$\begin{aligned}C_{delay} = [(1 - e^{-(C_T T_{x,PC}/\tau_{x,AC})}) \cdot (1 - e^{-(C_T T_{x,PC}/\tau_{x,TH})}) \cdot (1 - e^{-(C_T T_{y,PC}/\tau_{x,MI})}) \cdot (1 - e^{-(C_T T_{y,PC}/\tau_{y,AC})}) \cdot (1 - e^{-(C_T T_{y,PC}/\tau_{y,TH})}) \\ \cdot (1 - e^{-(C_T T_{y,PC}/\tau_{y,MI})}) \cdot (1 - e^{-(C_T T_{z,PC}/\tau_{z,AC})}) \cdot (1 - e^{-(C_T T_{z,PC}/\tau_{z,TH})}) \cdot (1 - e^{-(C_T T_{z,PC}/\tau_{z,MI})})]^{1/3}\end{aligned} \tag{A.15}$$

References

[1] G.W. Ehrenstein, G. Riedel, P. Trawiel, Thermal Analysis of Plastics: Theory and Practice, Carl Hanser Verlag, 2004.
[2] T. Hatakeyama, F.X. Quinn, Thermal Analysis: Fundamentals and Applications to Polymer Science, John Wiley & Sons, 1994.
[3] S.M. Hasnain, Energy Convers. Manage. 39 (11) (1998) 1127–1138.
[4] E.L. Charsley, P.G. Laye, V. Palakollu, J.J. Rooney, B. Joseph, Thermochim. Acta 446 (2006) 29–32.
[5] J.A. Martins, J.J.C. Cruz-Pinto, Thermochim. Acta 332 (1999) 179–188.
[6] R. Androsch, B. Wunderlich, Thermochim. Acta 369 (2001) 62–78.
[7] H. Huth, M. Beiner, S. Weyer, M. Merziyakov, C. Schick, E. Donth, Thermochim. Acta 377 (2001) 113–124.
[8] ISO 11357-1:1997, Differential Scanning Calorimetry (DSC). Part 1. General Principles; 1997.
[9] ISO 11357-3:1999, Differential Scanning Calorimetry (DSC). Part 3. Determination of Temperature and Enthalpy of Melting and Crystallization; 1999.
[10] G.W.H. Höhne, H.K. Cammenga, W. Eysel, E. Gmelin, W. Hemminger, Thermochim. Acta 160 (1990) 1–12.
[11] R.C. Weast, CRC Handbook of Chemistry and Physics, 1st student ed., CRC press, 1988.
[12] G. Arfken, Mathematical Methods for Physicists, 3rd ed., 1985, p. 928.